Electronic Supplementary Information (ESI†)

for

Enhancing the photocytotoxic potential of curcumin on terpyridyl lanthanide(III) complex formation

Akhtar Hussain,[a] Kumar Somyajit,[b] Bhabatosh Banik,[a] Samya Banerjee,[a] Ganesh Nagaraju*[b] and Akhil R. Chakravarty*[a]

[a] *Department of Inorganic and Physical Chemistry, Indian Institute of Science, Bangalore-560 012, India. E-mail: arc@ipc.iisc.ernet.in; Tel: +91-80-22932533*

[b] *Department of Biochemistry, Indian Institute of Science, Bangalore-560 012, India. E-mail:* nganesh@biochem.iisc.ernet.in*; Tel:* +91-80-22933055

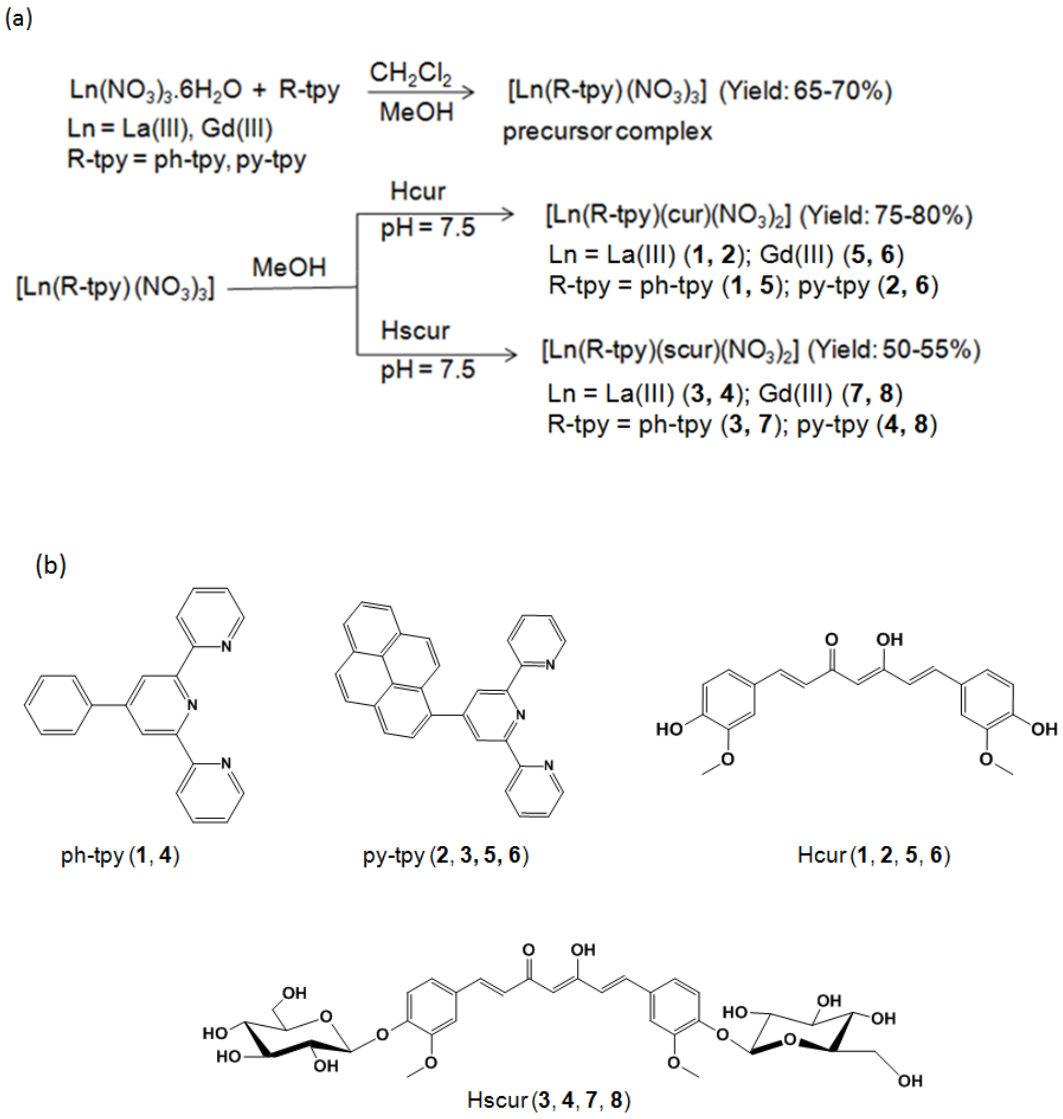

Fig. S1 Generalized synthetic scheme for (a) the lanthanide(III) complexes **1**-**8** and (b) the ligands used in the present study.

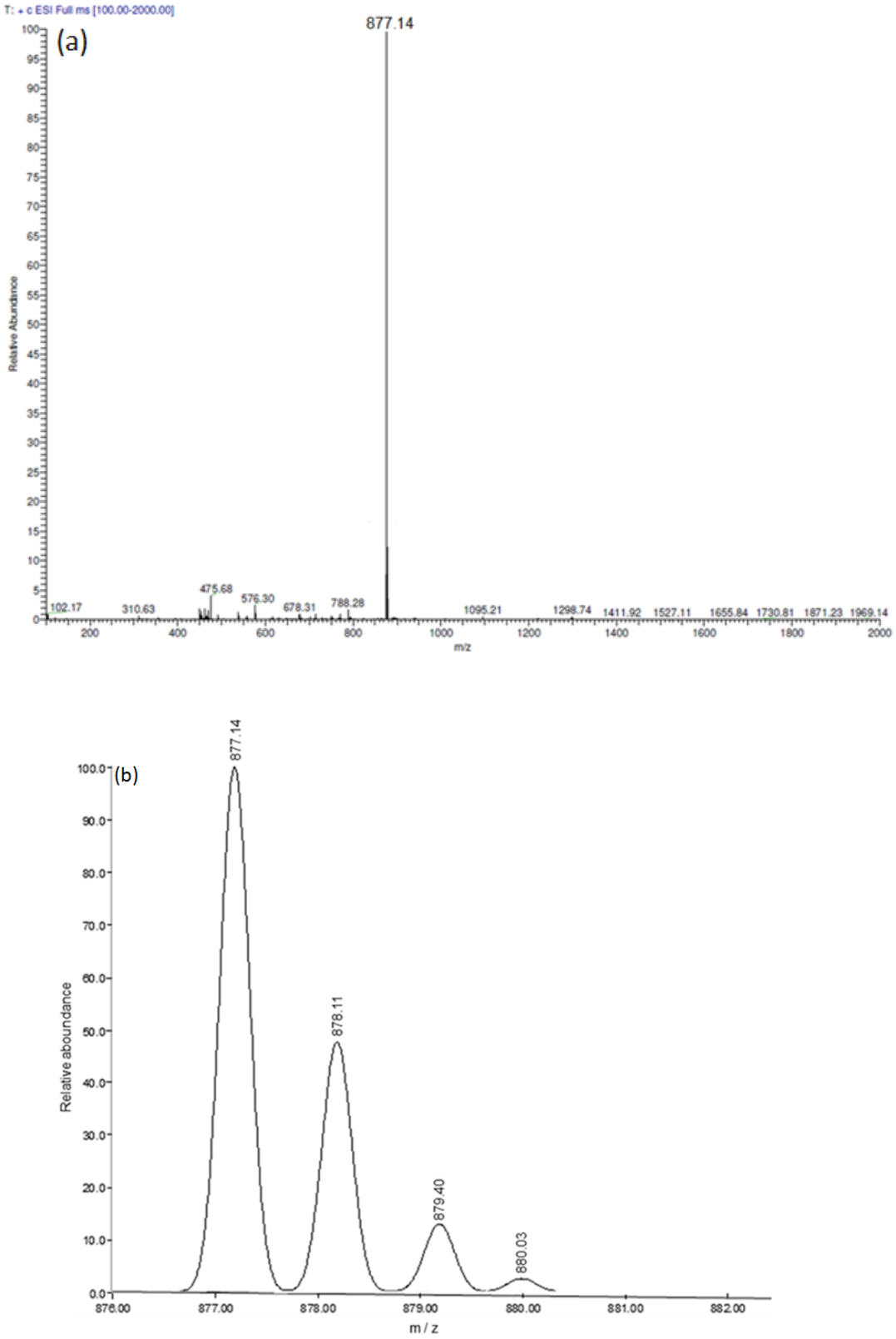

Fig. S2 (a) The ESI-MS spectrum and (b) the isotopic distribution pattern of [La(ph-tpy)(cur)$(NO_3)_2$] (**1**) in 10% aqueous MeOH showing the prominent [M-(NO_3^-)]$^+$ peak.

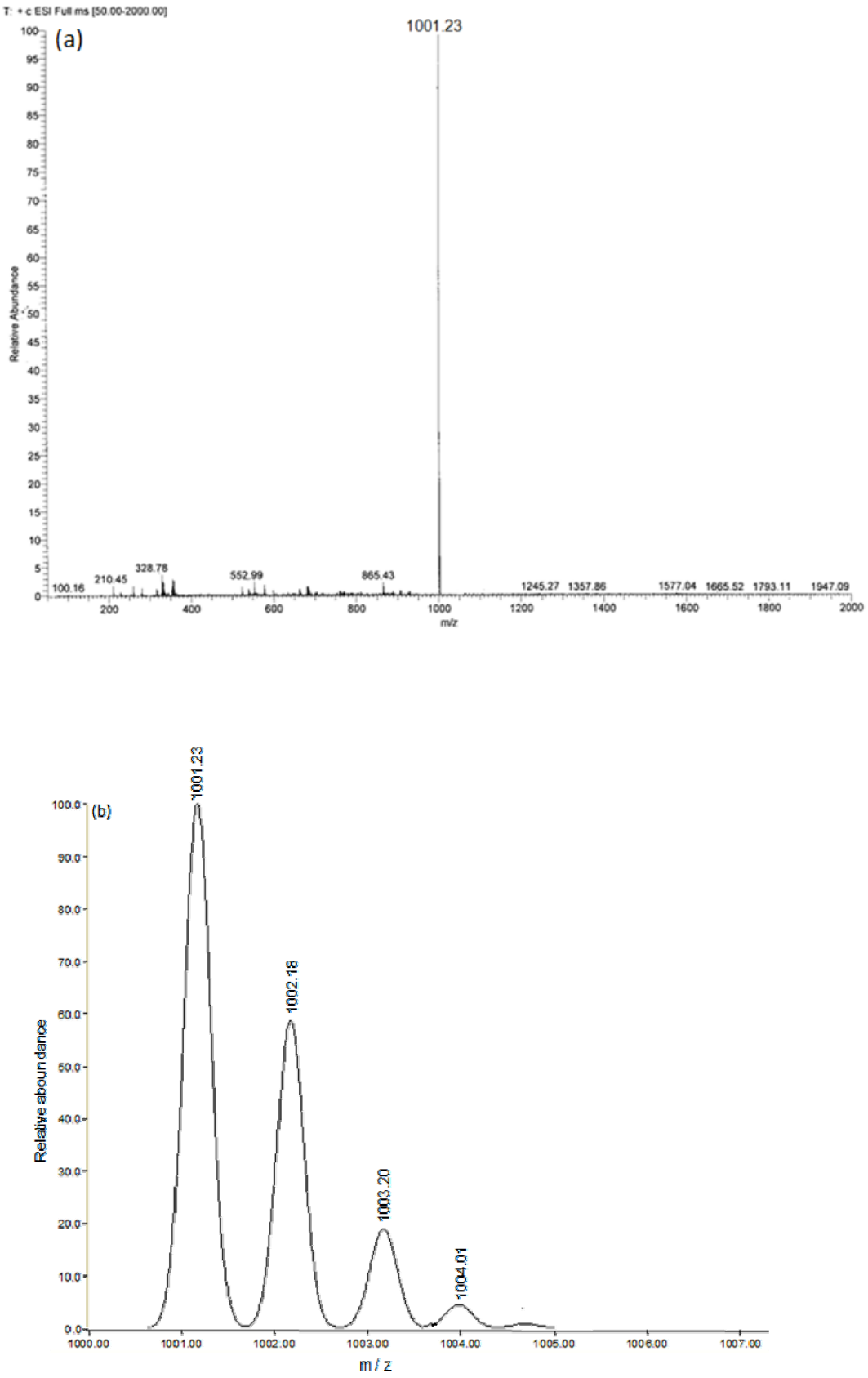

Fig. S3 (a) The ESI-MS spectrum and (b) the isotopic distribution pattern of [La(py-tpy)(cur)$(NO_3)_2$] (**2**) in 10% aqueous MeOH showing the prominent $[M\text{-}(NO_3^-)]^+$ peak.

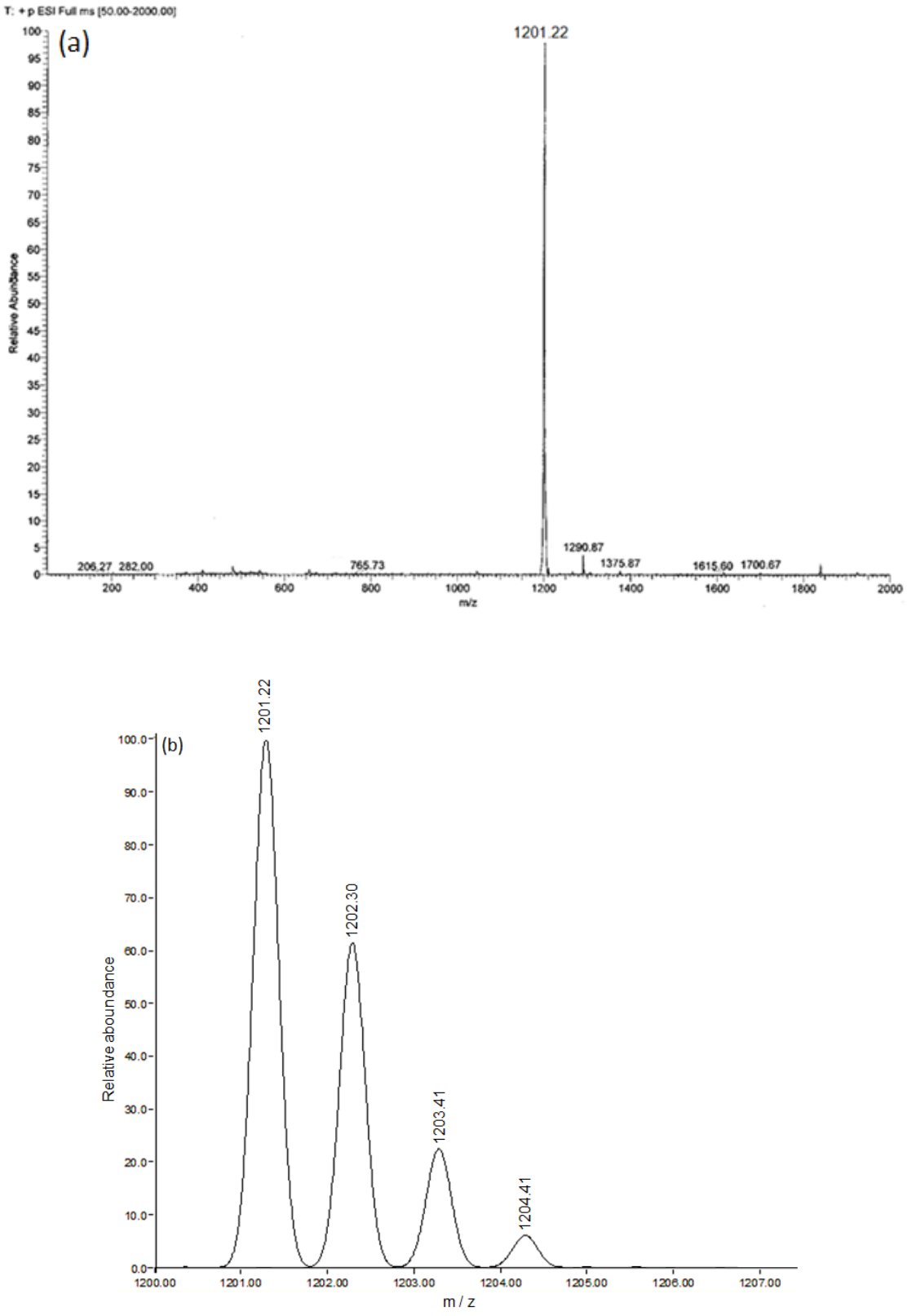

Fig. S4 (a) The ESI-MS spectrum and (b) the isotopic distribution pattern of [La(phtpy)(scur)$(NO_3)_2$] (**3**) in 10% aqueous MeOH showing the prominent $[M-(NO_3^-)]^+$ peak.

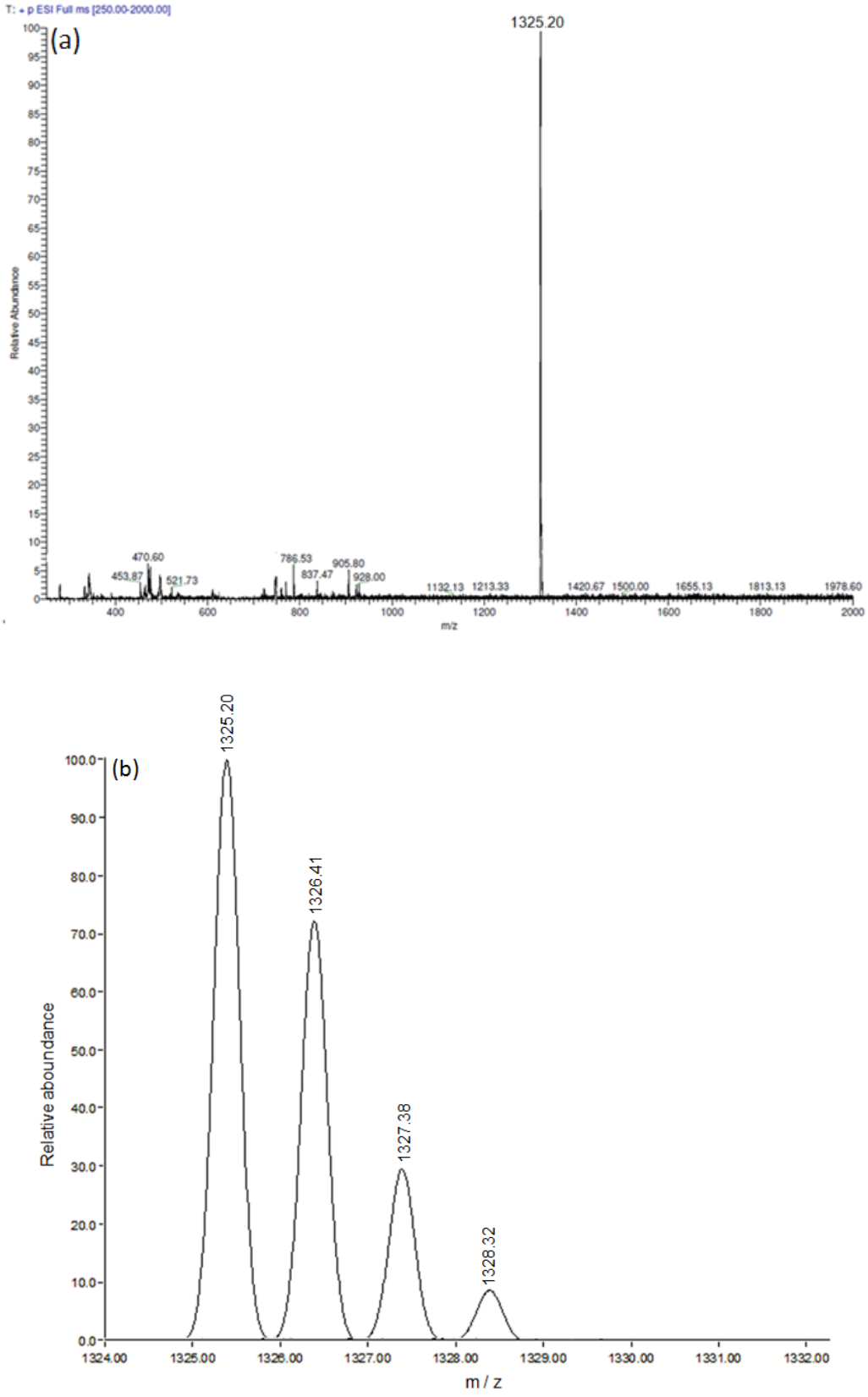

Fig. S5 (a) The ESI-MS spectrum and (b) the isotopic distribution pattern of [La(py-tpy)(scur)(NO_3)$_2$] (**4**) in 10% aqueous MeOH showing the prominent [M-(NO_3^-)]$^+$ peak.

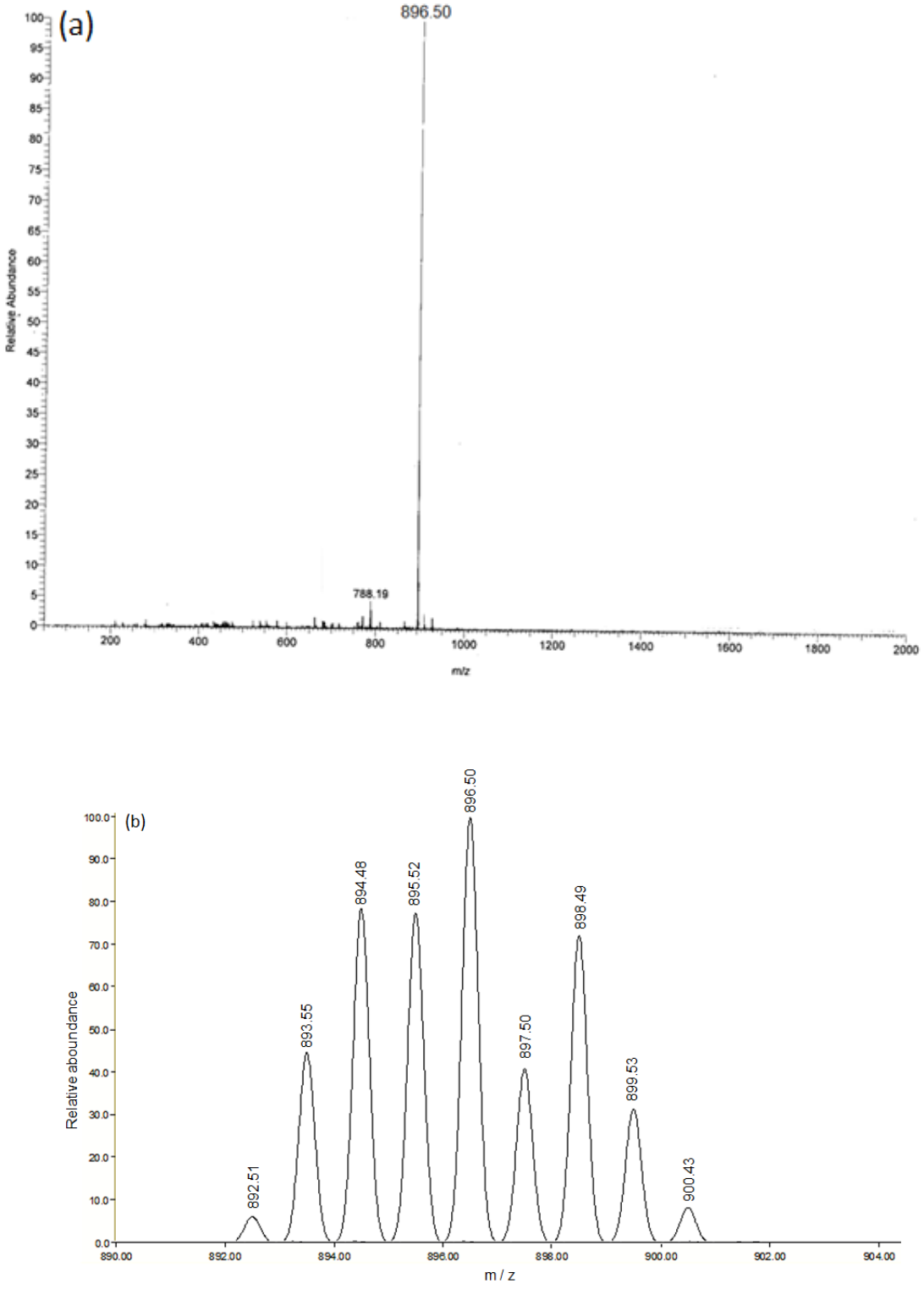

Fig. S6 (a) The ESI-MS spectrum and (b) the isotopic distribution pattern of [Gd(phtpy)(cur)$(NO_3)_2$] (**5**) in 10% aqueous MeOH showing the prominent $[M\text{-}(NO_3^-)]^+$ peak.

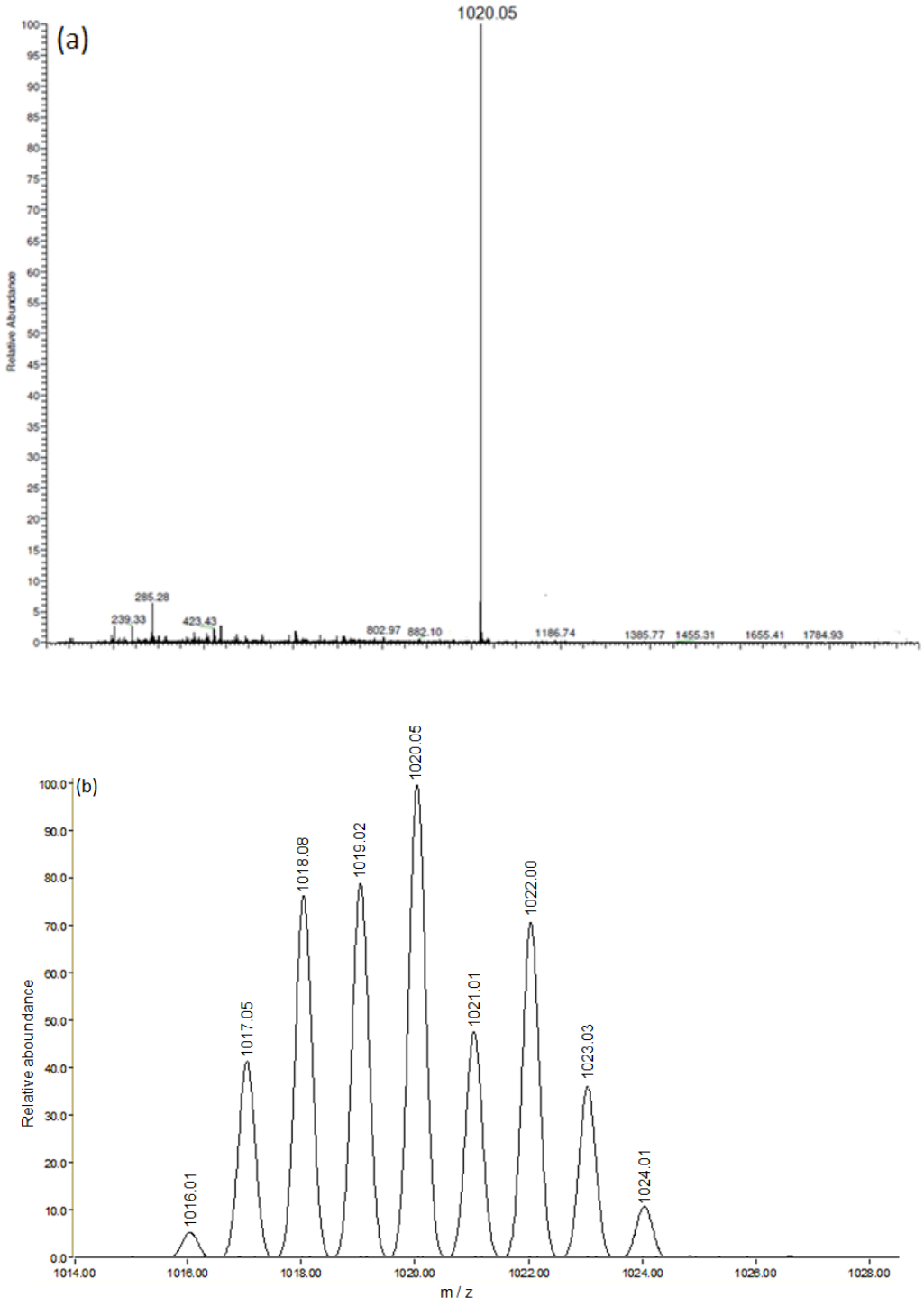

Fig. S7 (a) The ESI-MS spectrum and (b) the isotopic distribution pattern of [Gd(py-tpy)(cur)$(NO_3)_2$] (**6**) in 10% aqueous MeOH showing the prominent $[M-(NO_3^-)]^+$ peak.

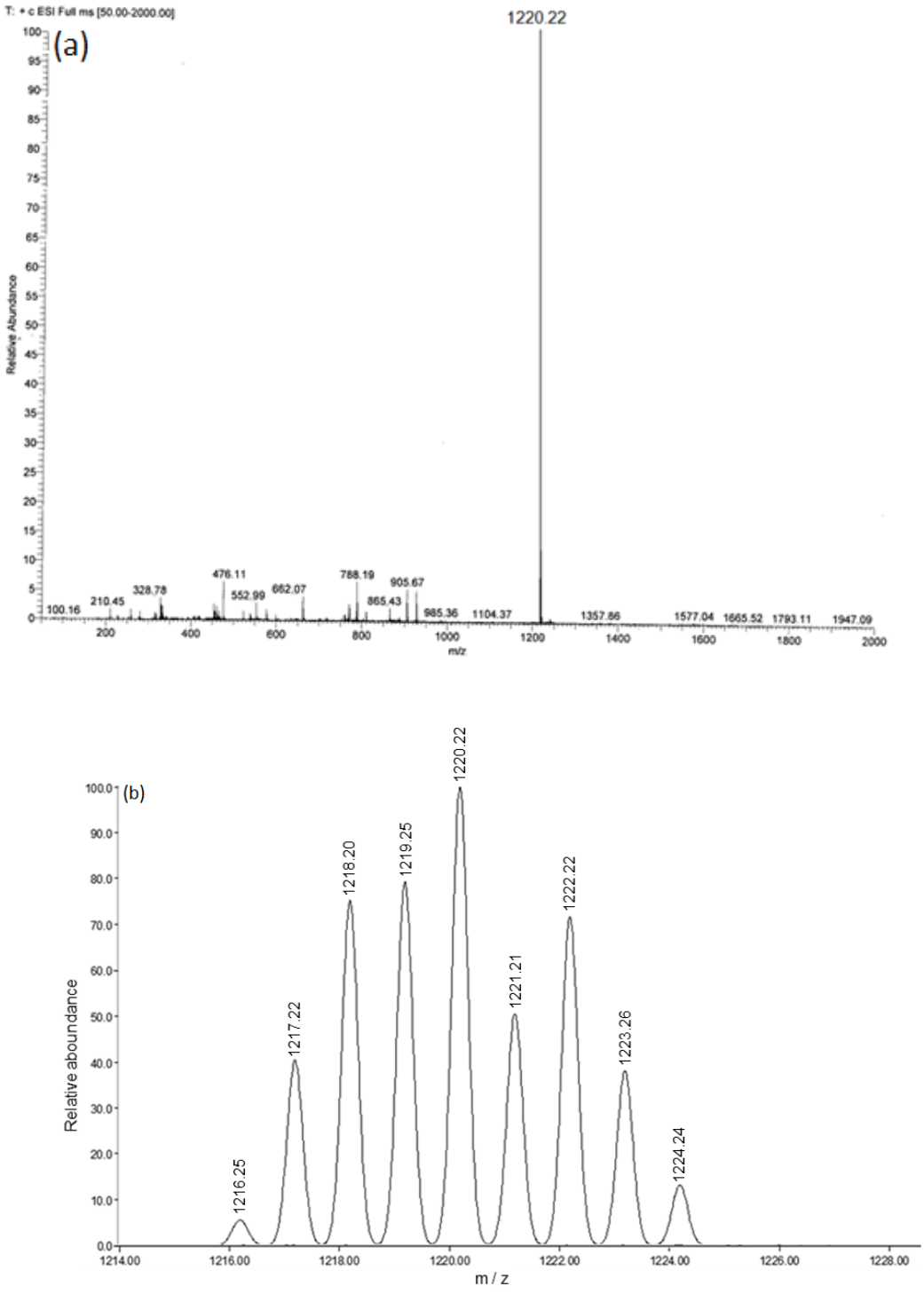

Fig. S8 (a) The ESI-MS spectrum and (b) the isotopic distribution pattern of [Gd(ph-tpy)(scur)$(NO_3)_2$] (**7**) in 10% aqueous MeOH showing the prominent $[M\text{-}(NO_3^-)]^+$ peak.

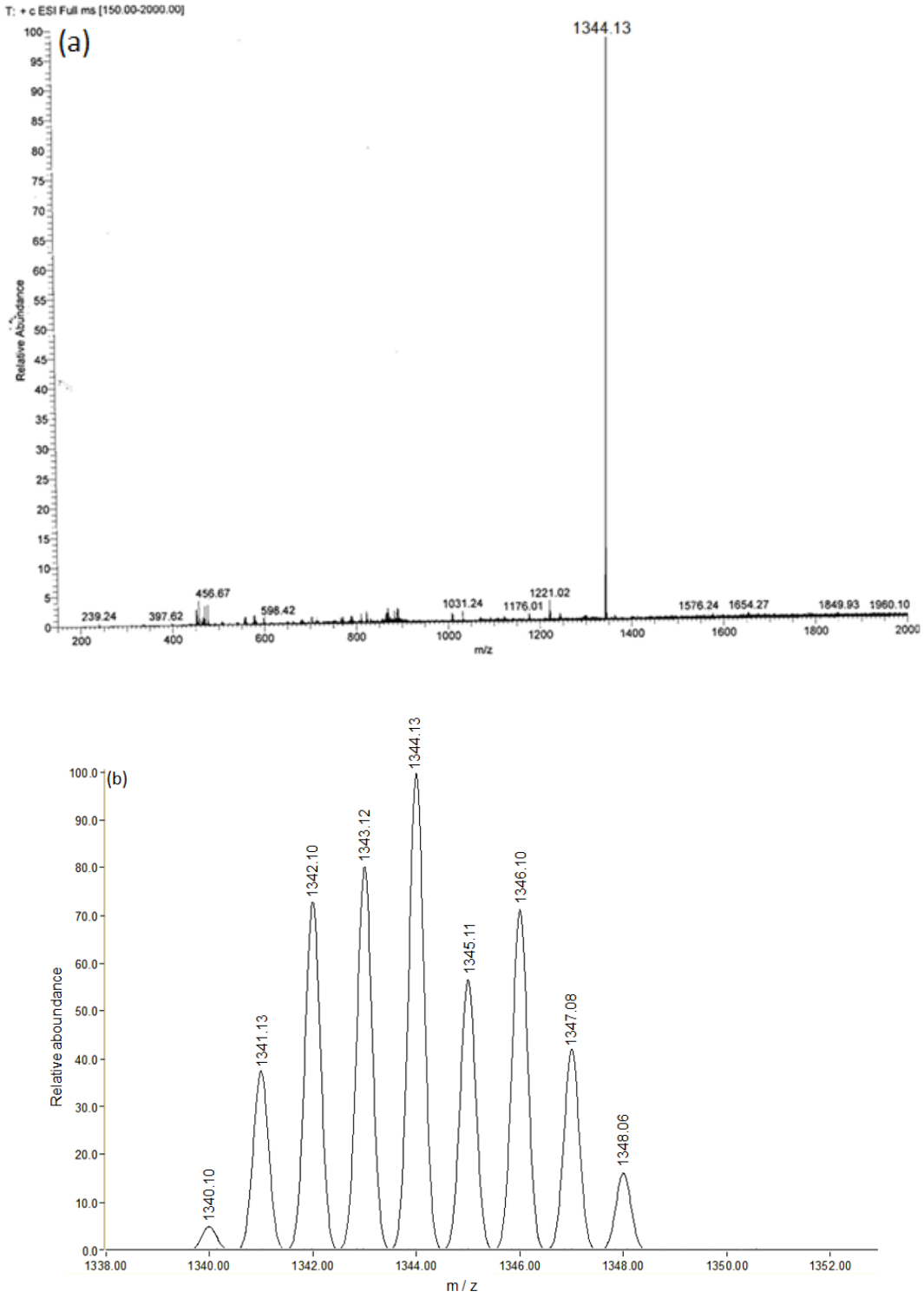

Fig. S9 (a) The ESI-MS spectrum and (b) the isotopic distribution pattern of [La(py-tpy)(scur)$(NO_3)_2$] (**8**) in 10% aqueous MeOH showing the prominent $[M\text{-}(NO_3^-)]^+$ peak.

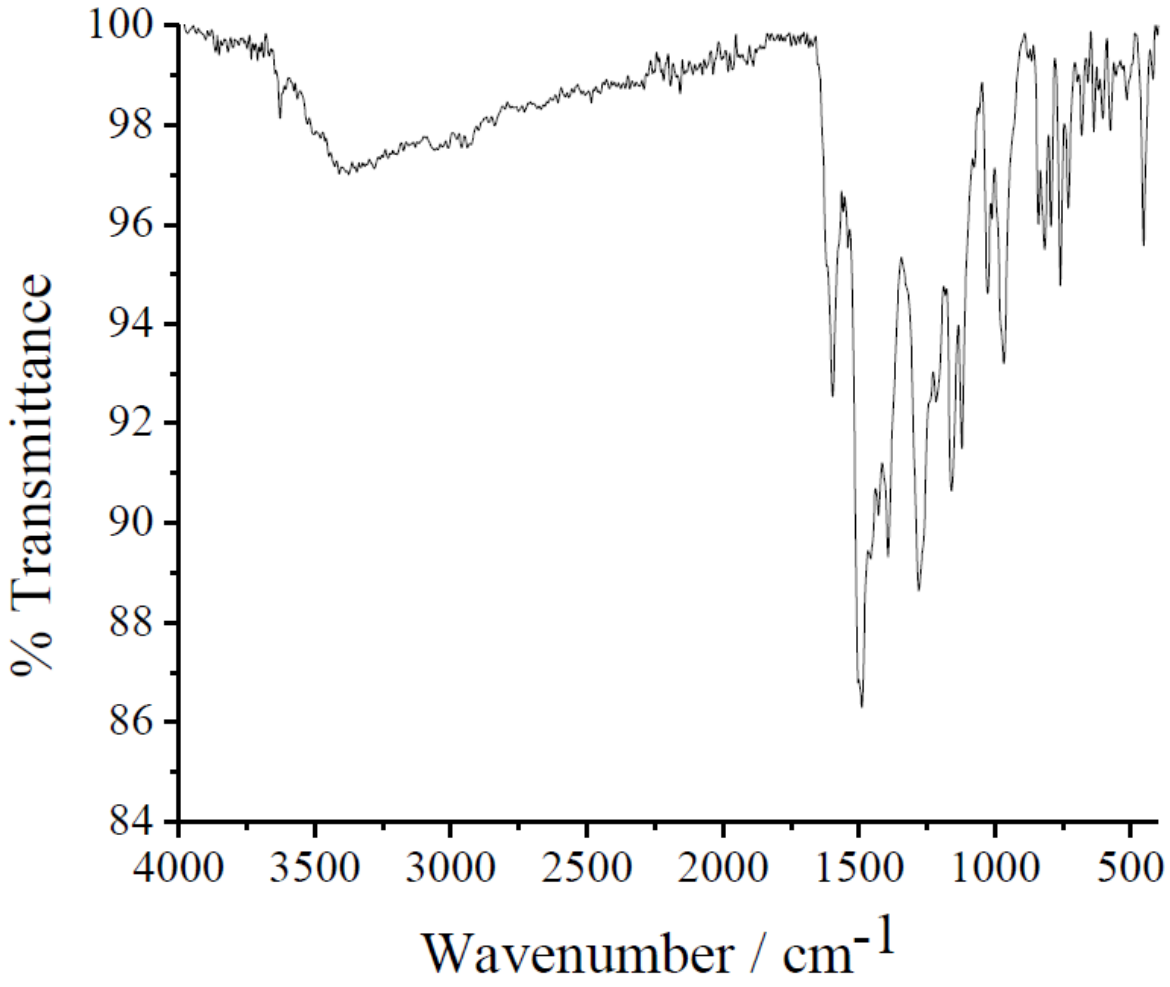

Fig. S10 IR spectrum of [La(ph-tpy)(cur)$(NO_3)_2$] (**1**).

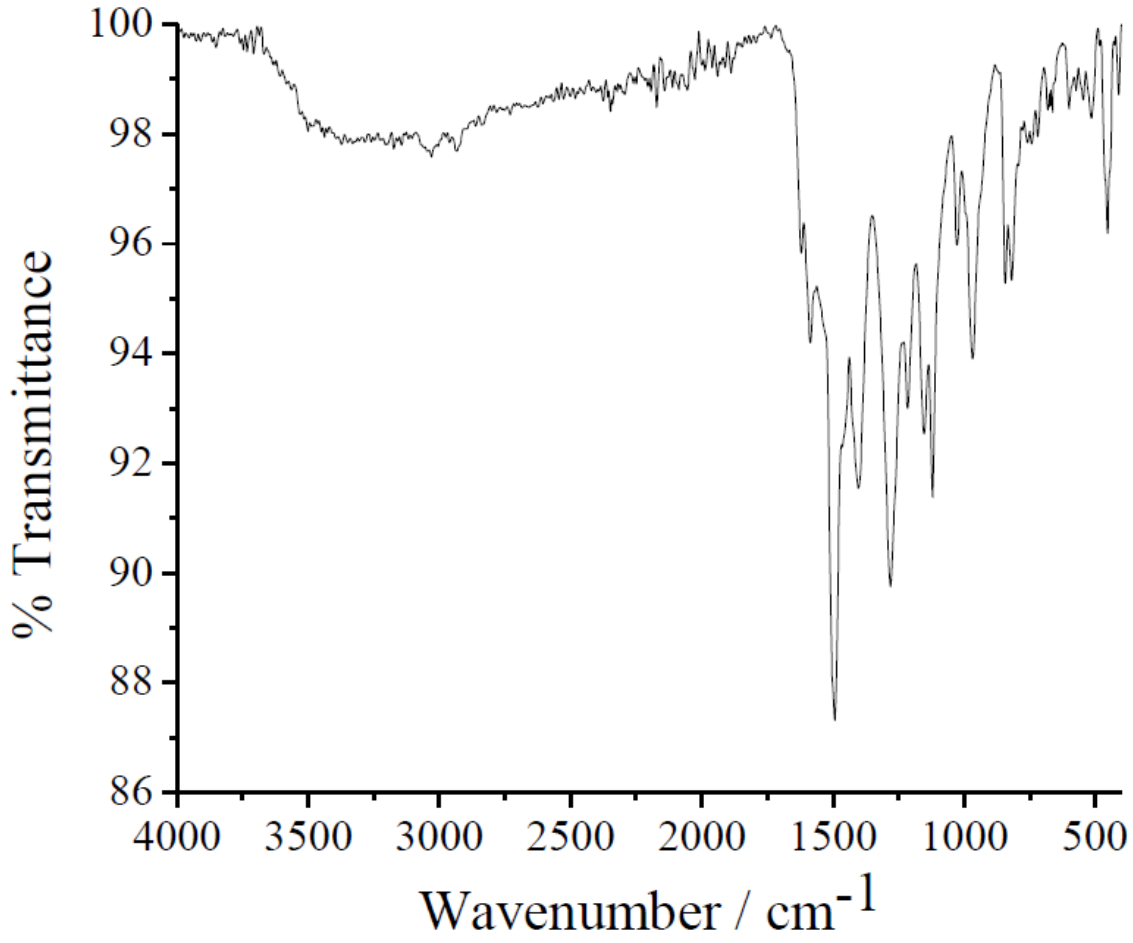

Fig. S11 IR spectrum of [La(py-tpy)(cur)$(NO_3)_2$] (**2**).

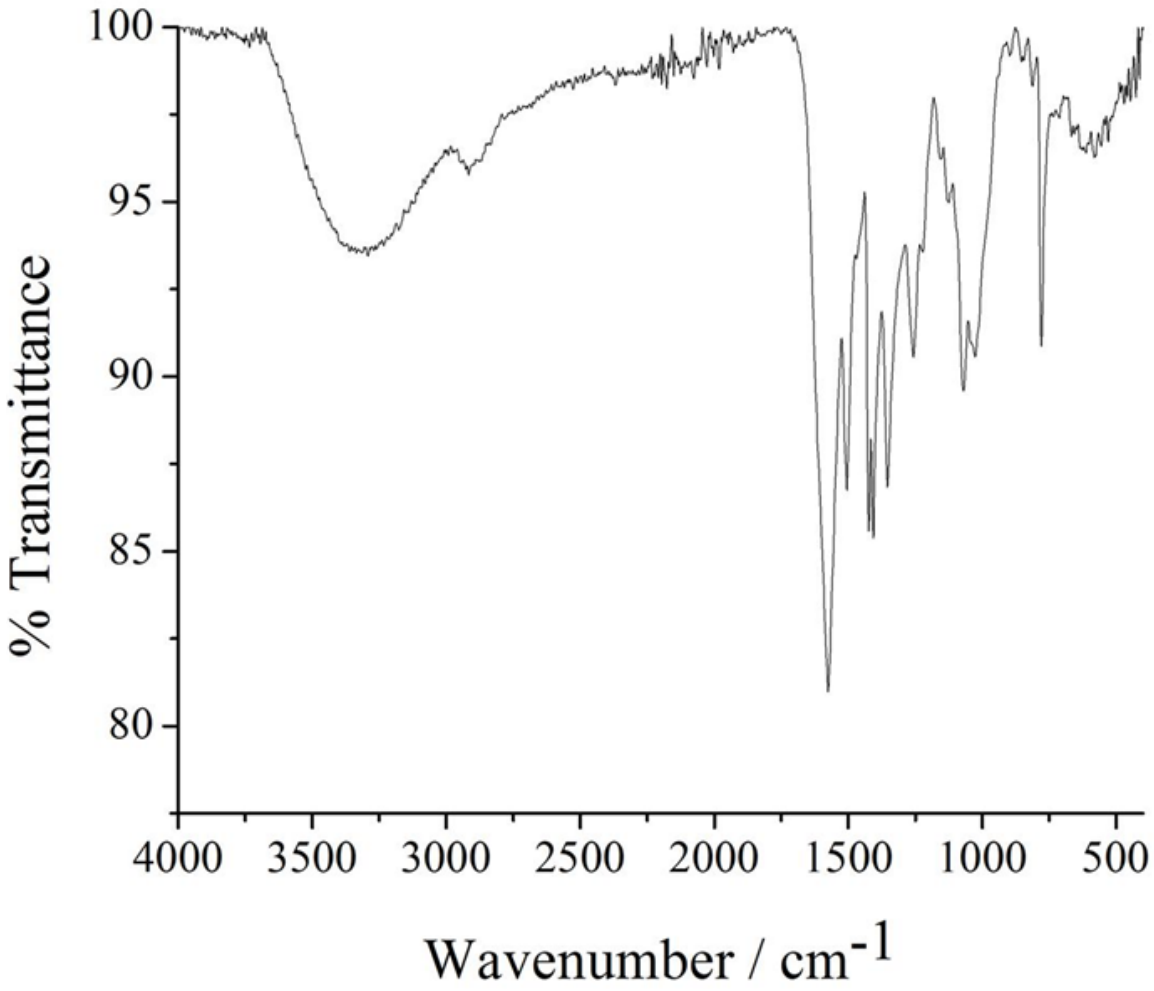

Fig. S12 IR spectrum of [La(ph-tpy)(scur)$(NO_3)_2$] (**3**).

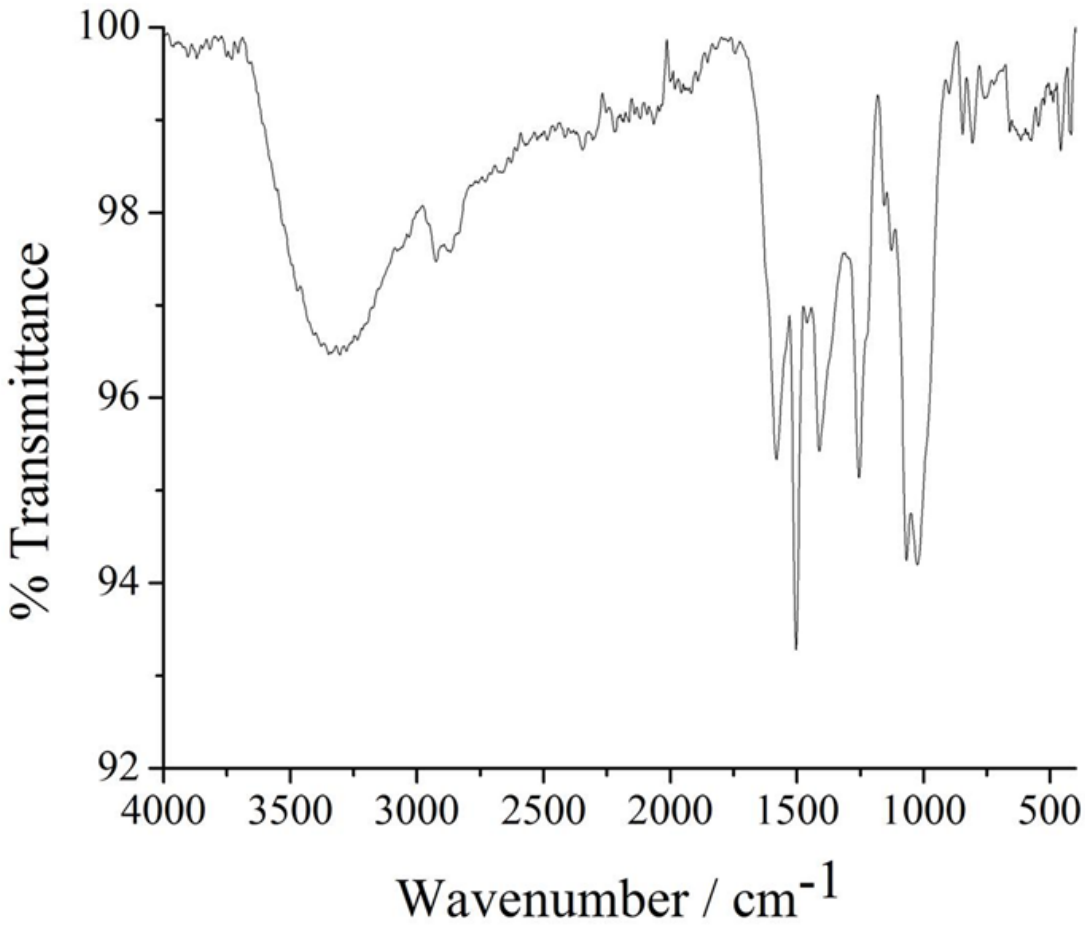

Fig. S13 IR spectrum of [La(py-tpy)(scur)$(NO_3)_2$] (**4**).

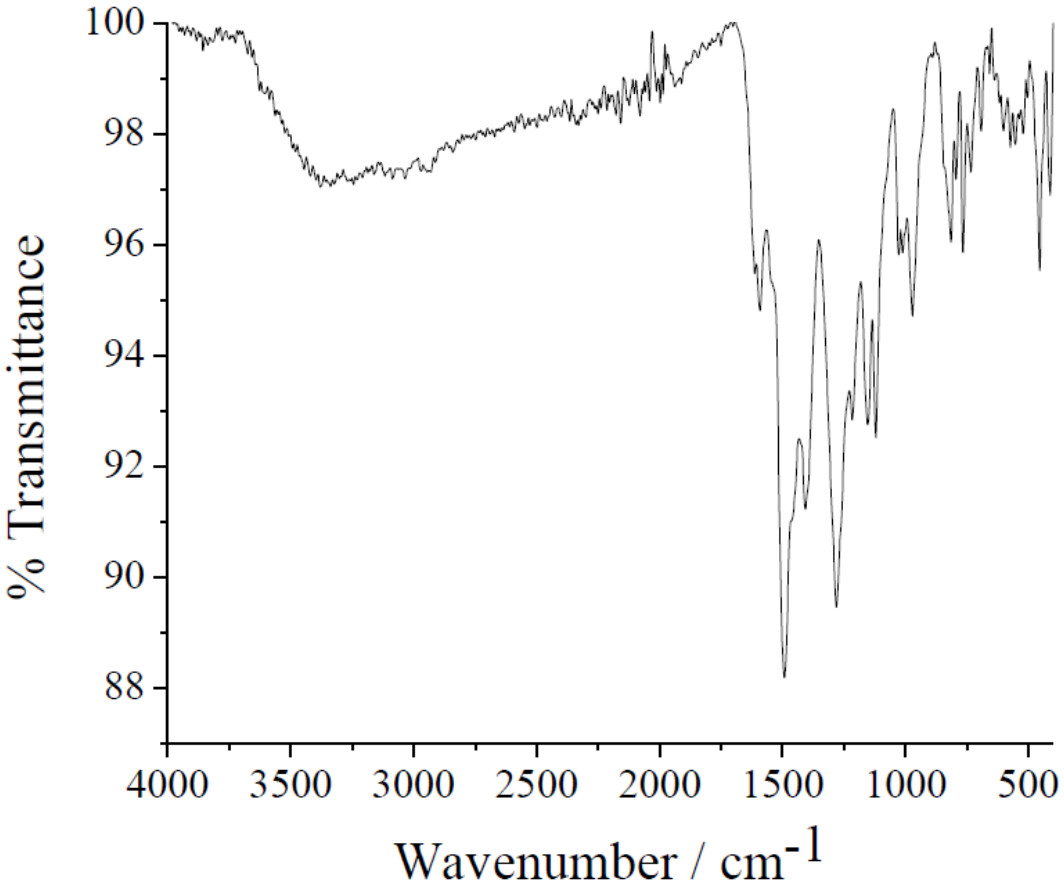

Fig. S14 IR spectrum of [Gd(ph-tpy)(cur)$(NO_3)_2$] (**5**).

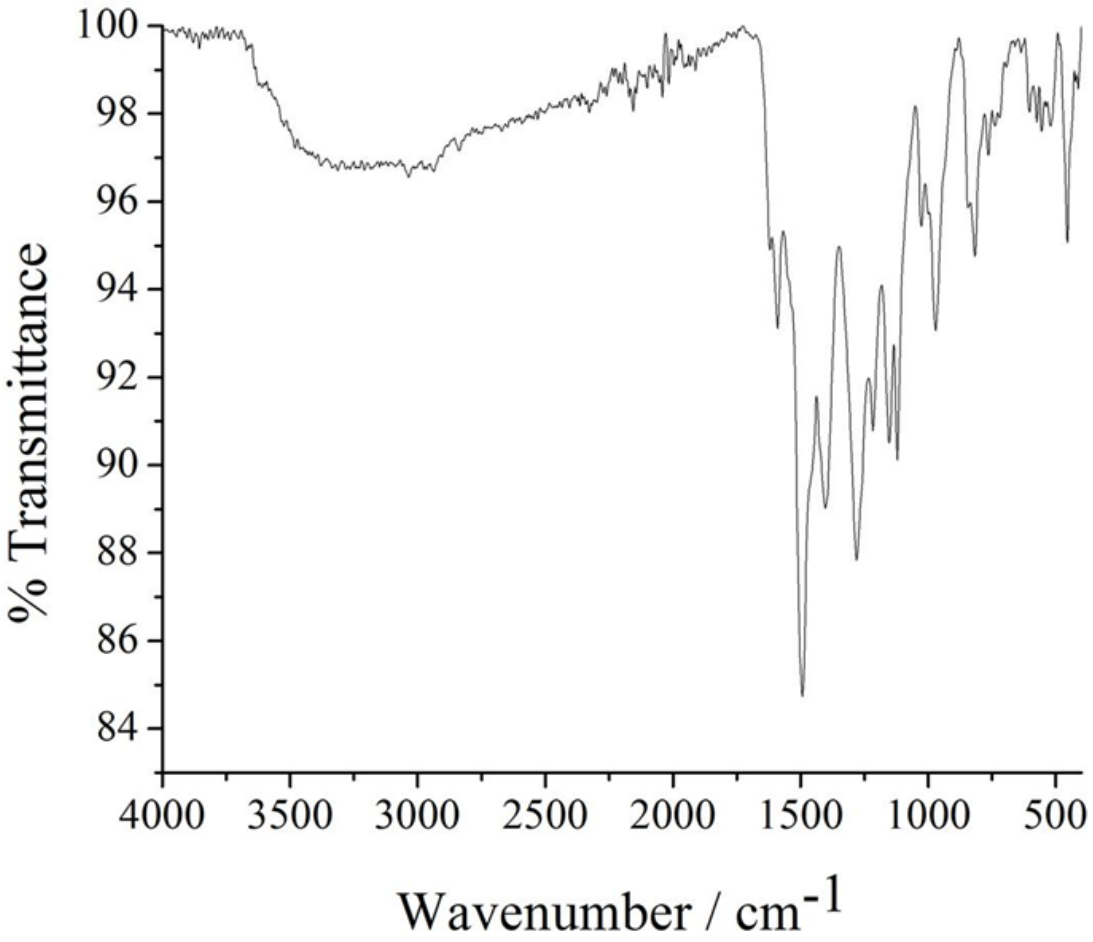

Fig. S15 IR spectrum of [Gd(py-tpy)(cur)$(NO_3)_2$] (**6**).

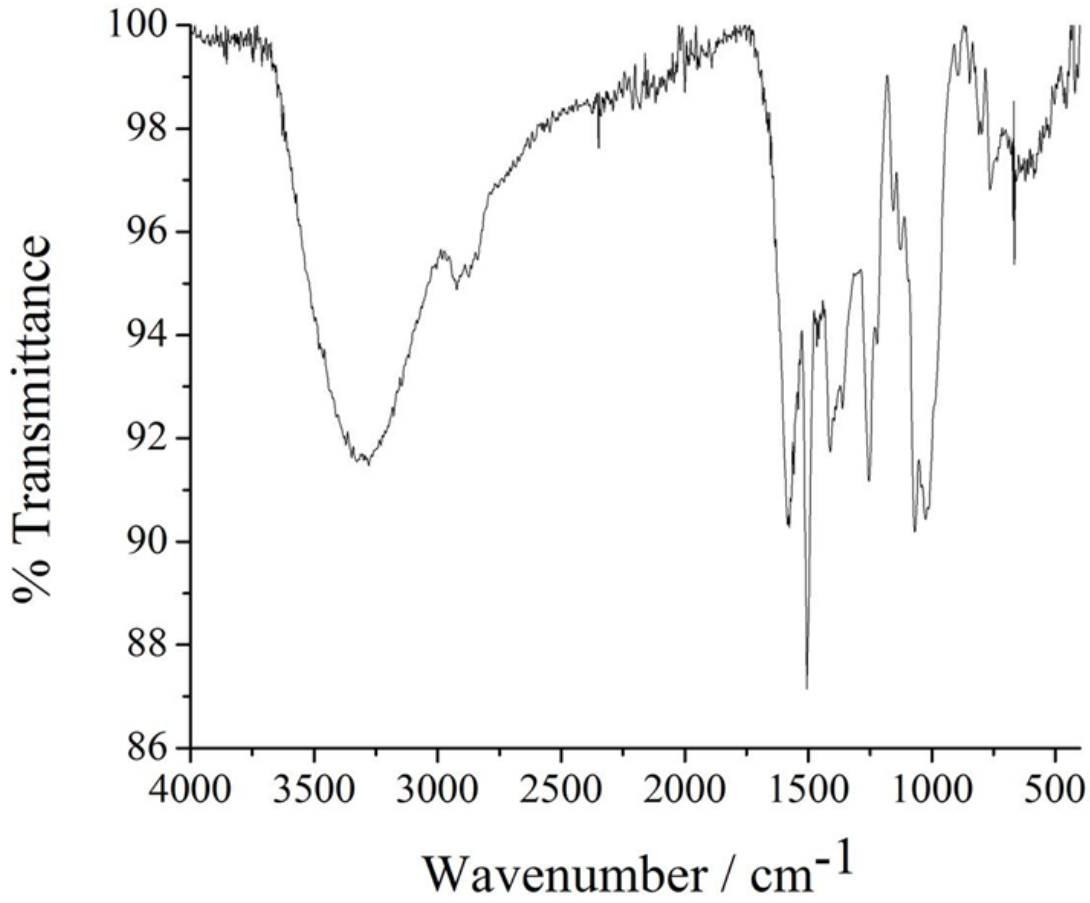

Fig. S16 IR spectrum of [Gd(ph-tpy)(scur)$(NO_3)_2$] (**7**).

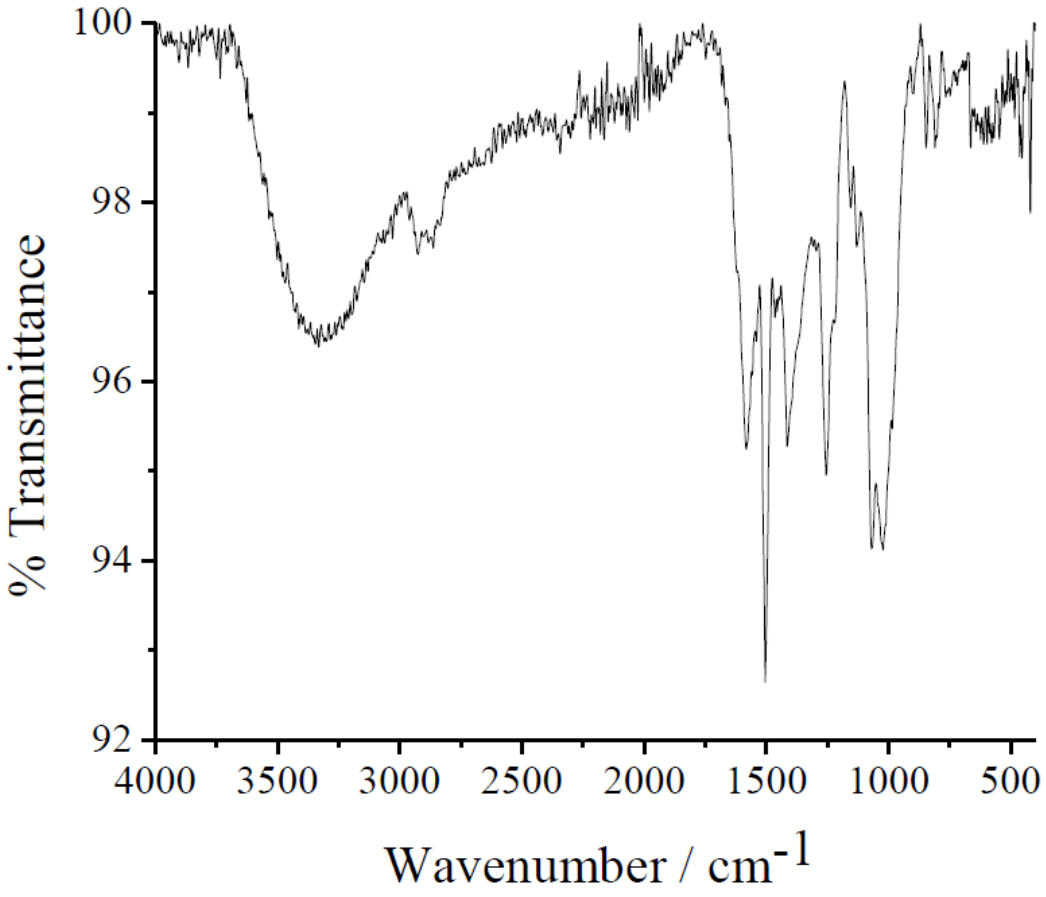

Fig. S17 IR spectrum of [Gd(py-tpy)(scur)$(NO_3)_2$] (**8**).

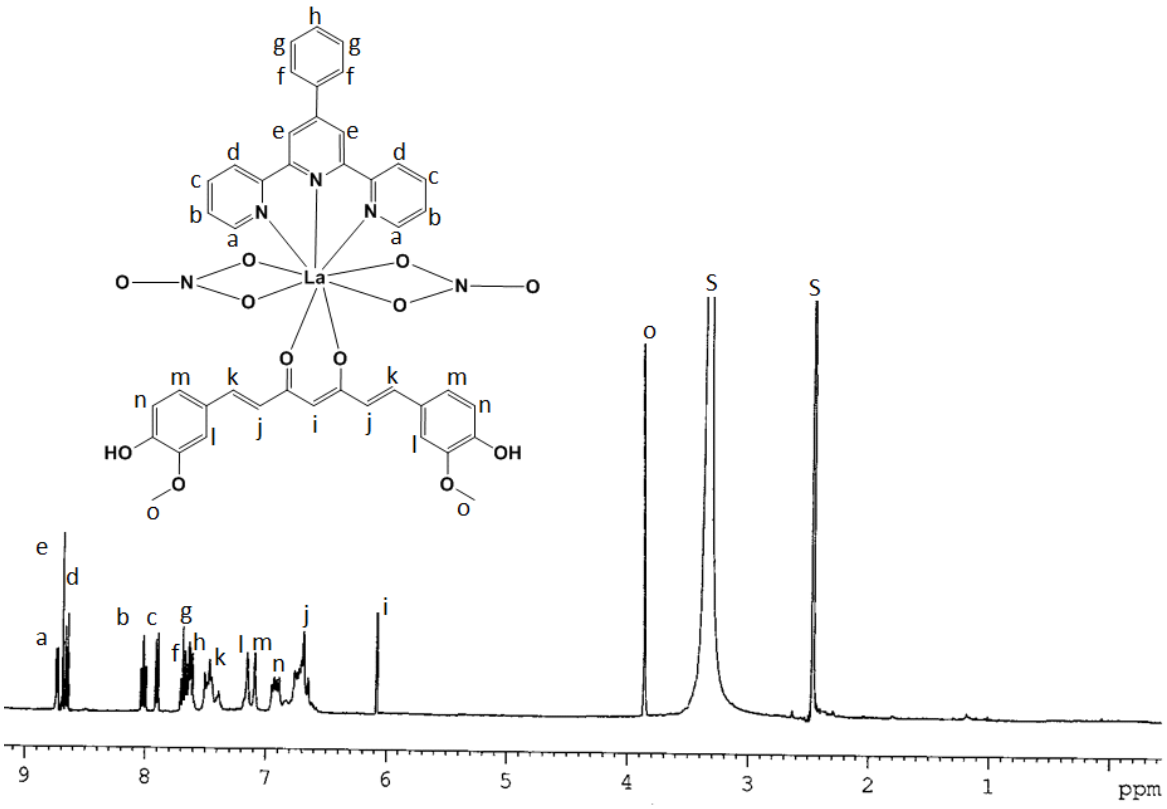

Fig. S18 ^{1}H NMR spectrum of [La(ph-tpy)(cur)$(NO_3)_2$] (**1**) in DMSO-d_6. The peaks marked S between 2-3.5 ppm are due to solvent.

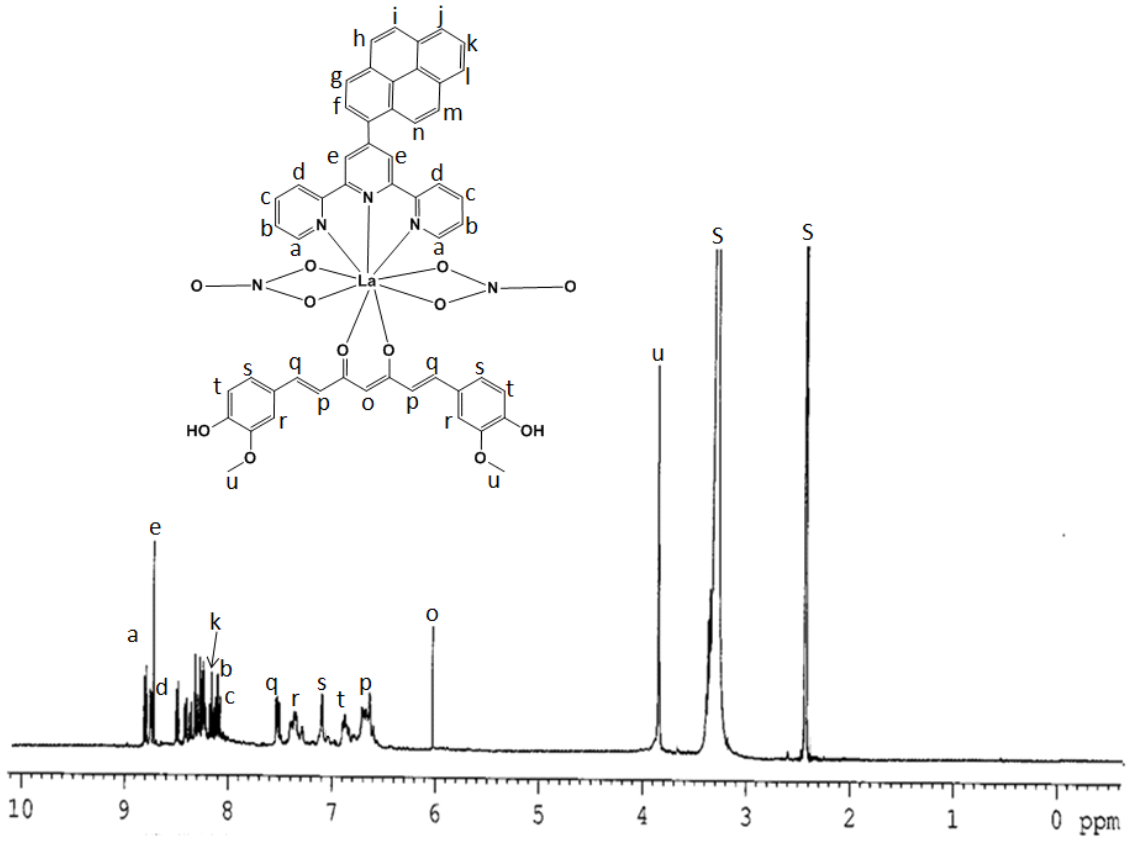

Fig. S19 ^{1}H NMR spectrum of [La(py-tpy)(cur)$(NO_3)_2$] (**2**) in DMSO-d_6. The peaks marked S between 2-3.5 ppm are due to solvent.

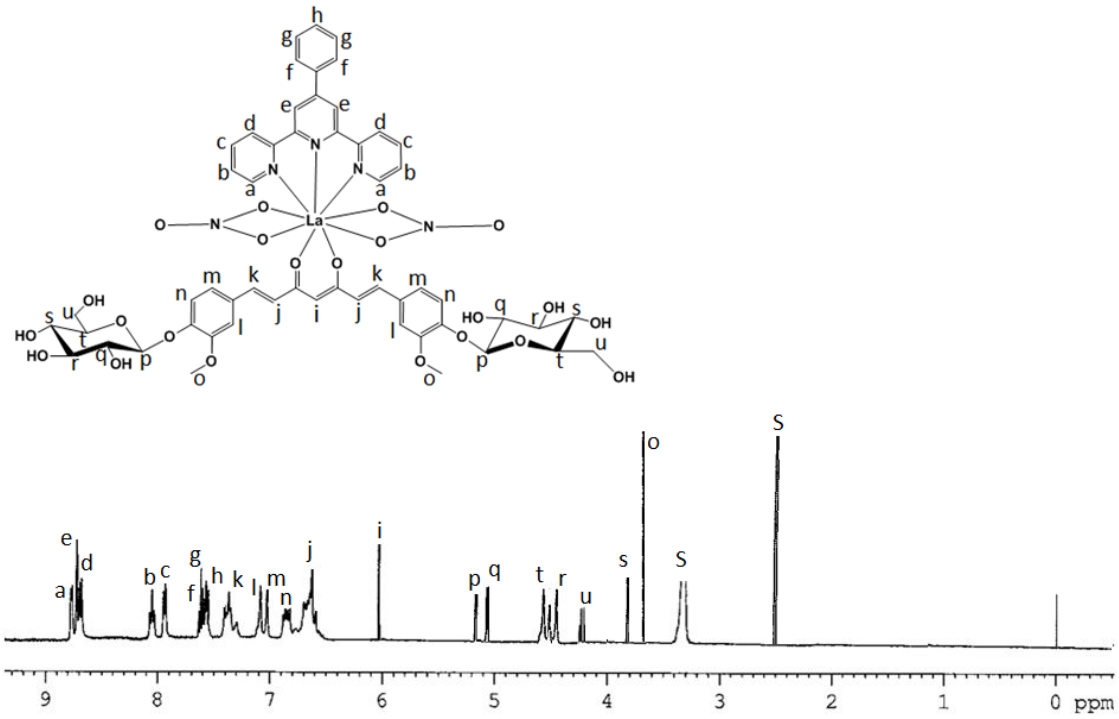

Fig. S20 ^{1}H-NMR spectrum of [La(ph-tpy)(scur)$(NO_3)_2$] (**3**) in DMSO-d_6. The peaks marked S between 2-3.5 ppm are due to solvent.

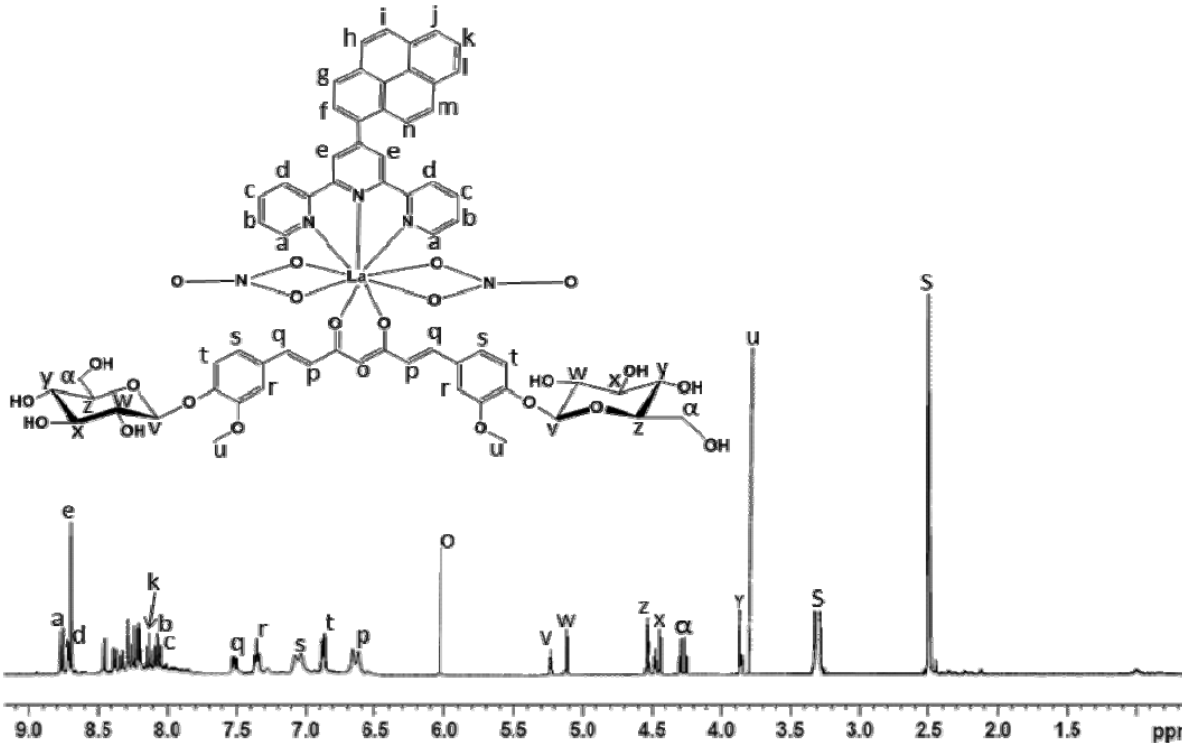

Fig. S21 ^{1}H-NMR spectrum of [La(py-tpy)(scur)$(NO_3)_2$] (**4**) in DMSO-d_6. The peaks marked S between 2-3.5 ppm are due to solvent.

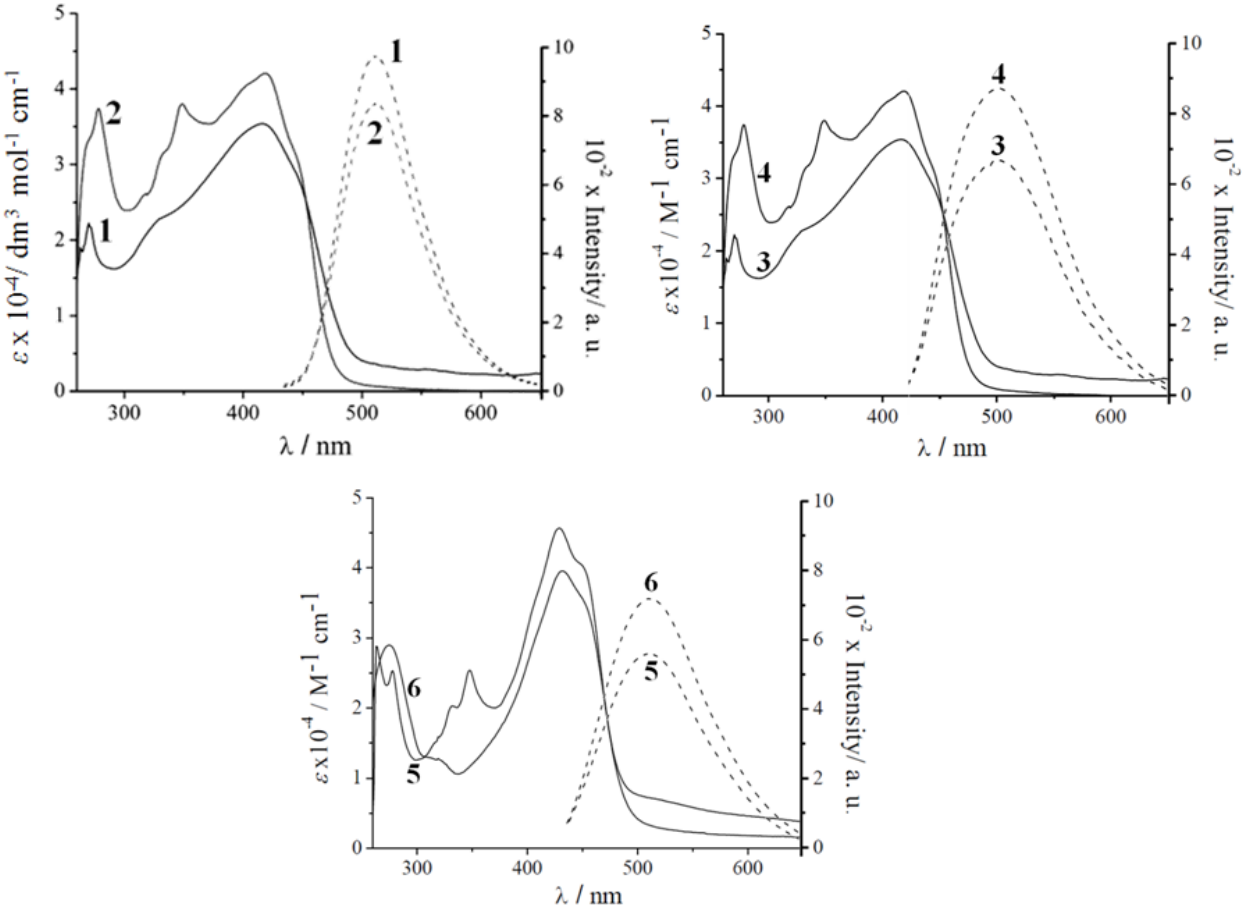

Fig. S22 The electronic absorption spectra of the complexes (a) **1** and **2**, (b) **3** and **4** and (c) **5** and **6** (solid curves) in 10% aqueous DMF. Fluorescence emission spectra of the complexes (a) **1** and **2**; (b) **3** and **4** and (c) **5** and **6** in 5% aqueous DMSO (dotted curves). The excitation wavelength is 420 nm.

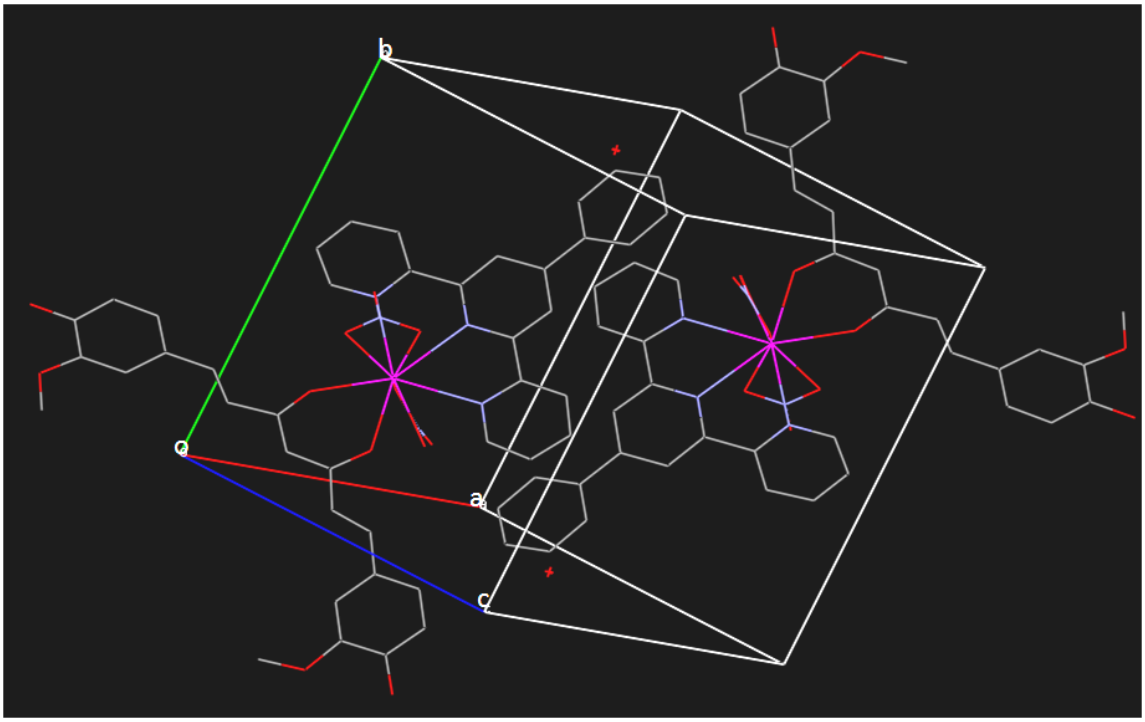

Fig. S23 Unit cell packing diagram of the complex [La(ph-tpy)(cur)(NO_3)$_2$].H_2O (**1**.H_2O).

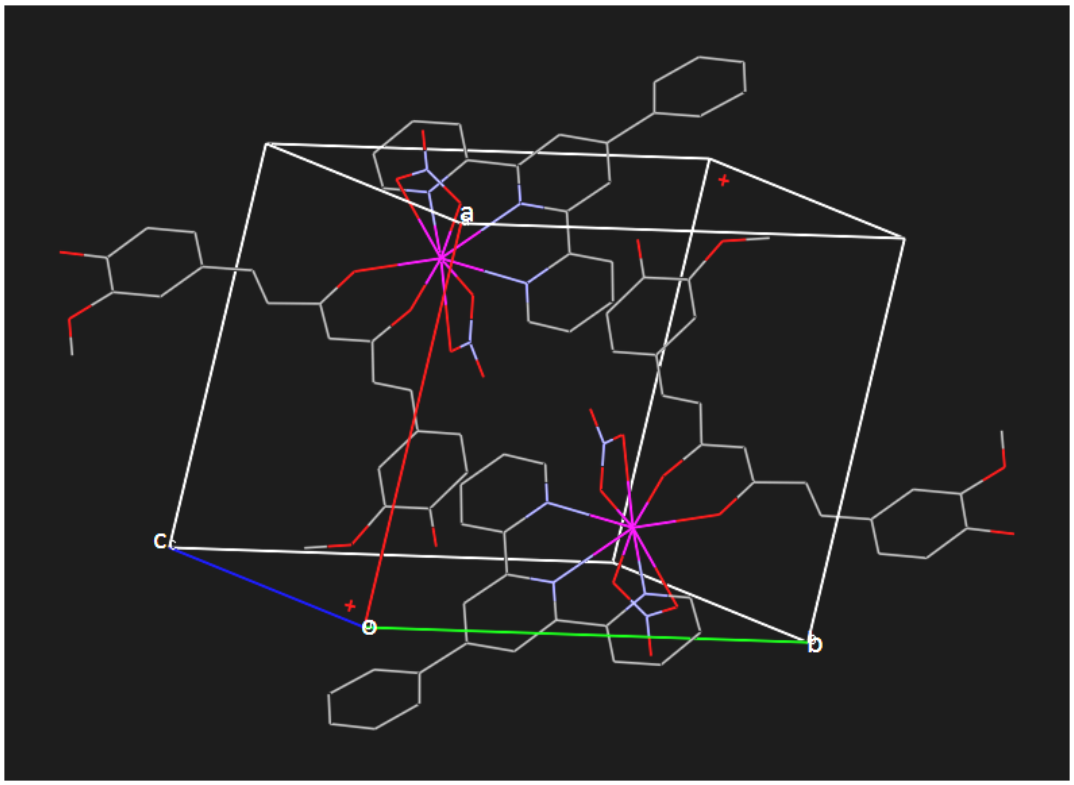

Fig. S24 Unit cell packing diagram of the complex [Gd(ph-tpy)(cur)$(NO_3)_2$].H_2O (**5**.H_2O).

Fig. 25 H- bonding (solid yellow lines) in the crystal lattice of $[La(ph\text{-}tpy)(cur)(NO_3)_2].H_2O$ (**1**.H_2O).

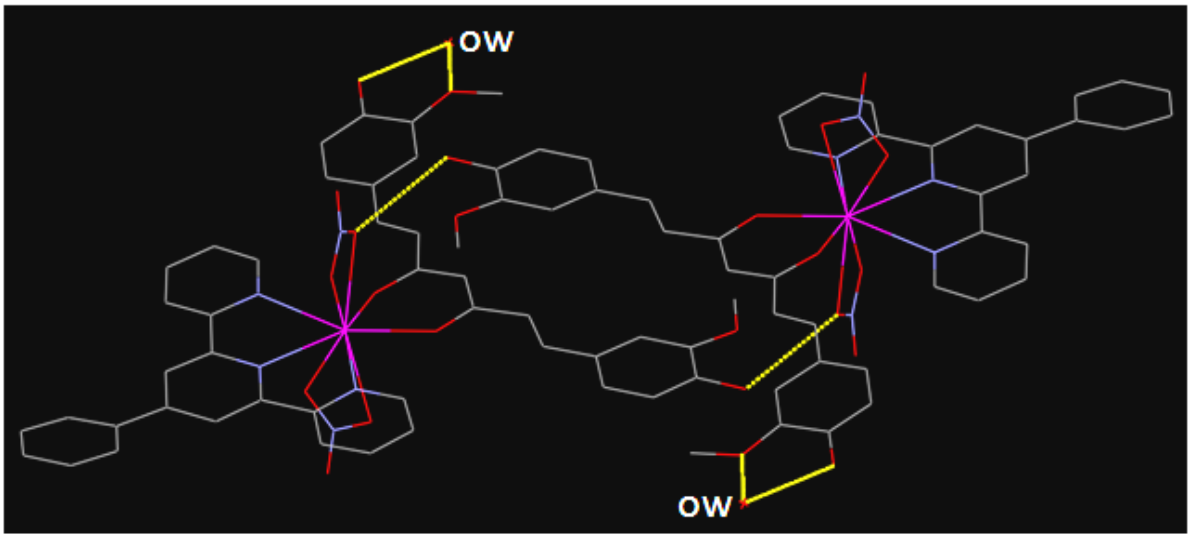

Fig. 26 H-bonding (solid yellow lines) in the crystal lattice of [Gd(ph-tpy)(cur)$(NO_3)_2$].H_2O (**5**.H_2O).

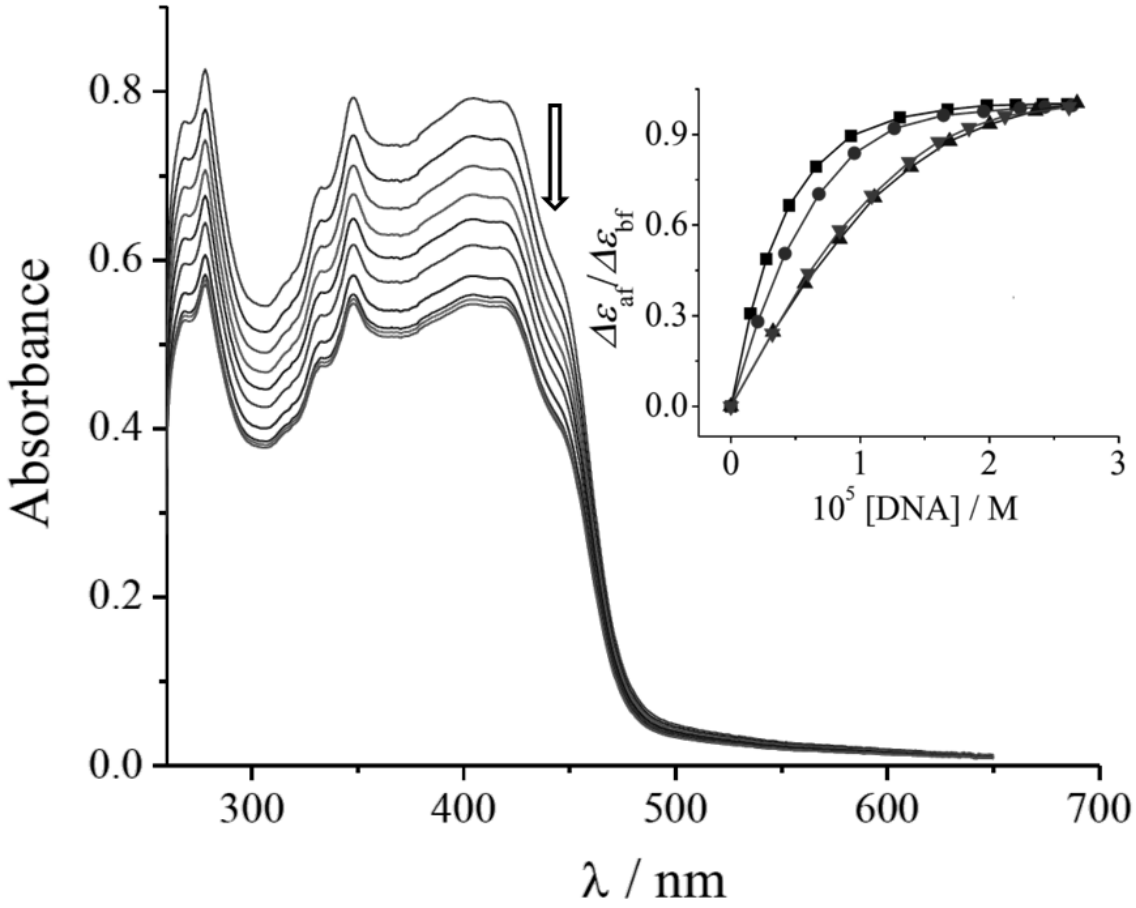

Fig. S27 Absorption spectral traces of complex **8** in 5 mM Tris-HCl buffer (pH 7.2) on increasing the quantity of calf thymus DNA. The inset shows the least-squares fit of $\Delta\varepsilon_{af}/\Delta\varepsilon_{bf}$ vs. [DNA] for [Gd(ph-tpy)(cur)$(NO_3)_2$] (**1**, ▲), [Gd(py-tpy)(cur)$(NO_3)_2$] (**2**, ■), [Gd(ph-tpy)(scur)$(NO_3)_2$] (**3**, ▼) and [Gd(py-tpy)(scur)$(NO_3)_2$] (**4**, ●).

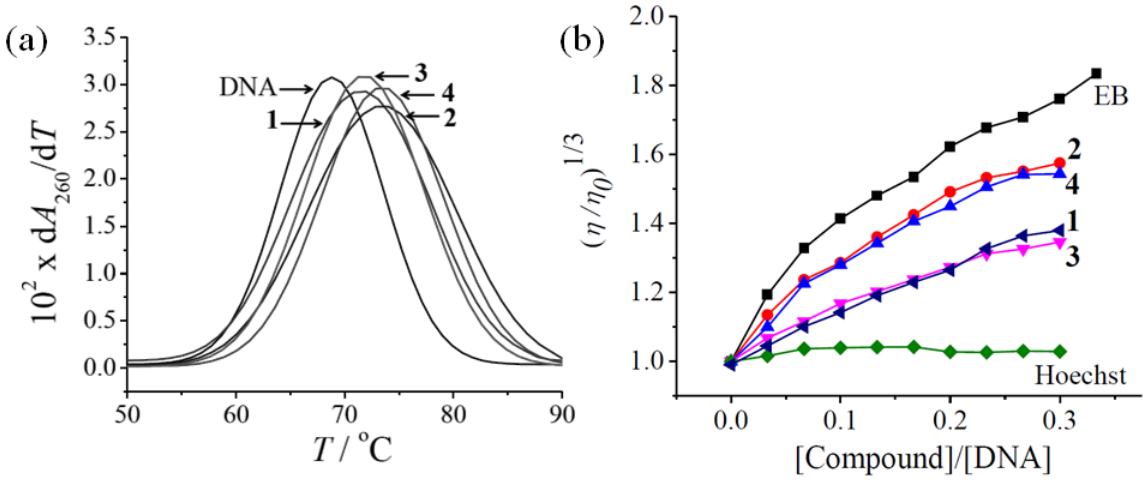

Fig. S28 (a) Derivative plots dA_{260}/dT vs. T for thermal denaturation of 180 μM calf thymus (ct) DNA alone and after addition of the complexes **1**–**4**. (b) Plots of $(\eta/\eta_0)^{1/3}$ vs. [compound]/[DNA] showing the effect of increasing concentration of the complexes [La(ph-tpy)(cur)$(NO_3)_2$] (**1**, ◀), [La(py-tpy)(cur)$(NO_3)_2$] (**2**, ●), [La(ph-tpy)(scur)$(NO_3)_2$] (**3**, ▼), [Gd(py-tpy)(scur)$(NO_3)_2$] (**4**, ▲), ethidium bromide (EB, ■) and Hoechst 33258 (♦) on the relative solution viscosities of ct-DNA at 37.0 (± 0.1) °C in 5 mM Tris-HCl buffer (pH 7.2) containing 2.5 – 20% DMF and 180 μM ct-DNA.

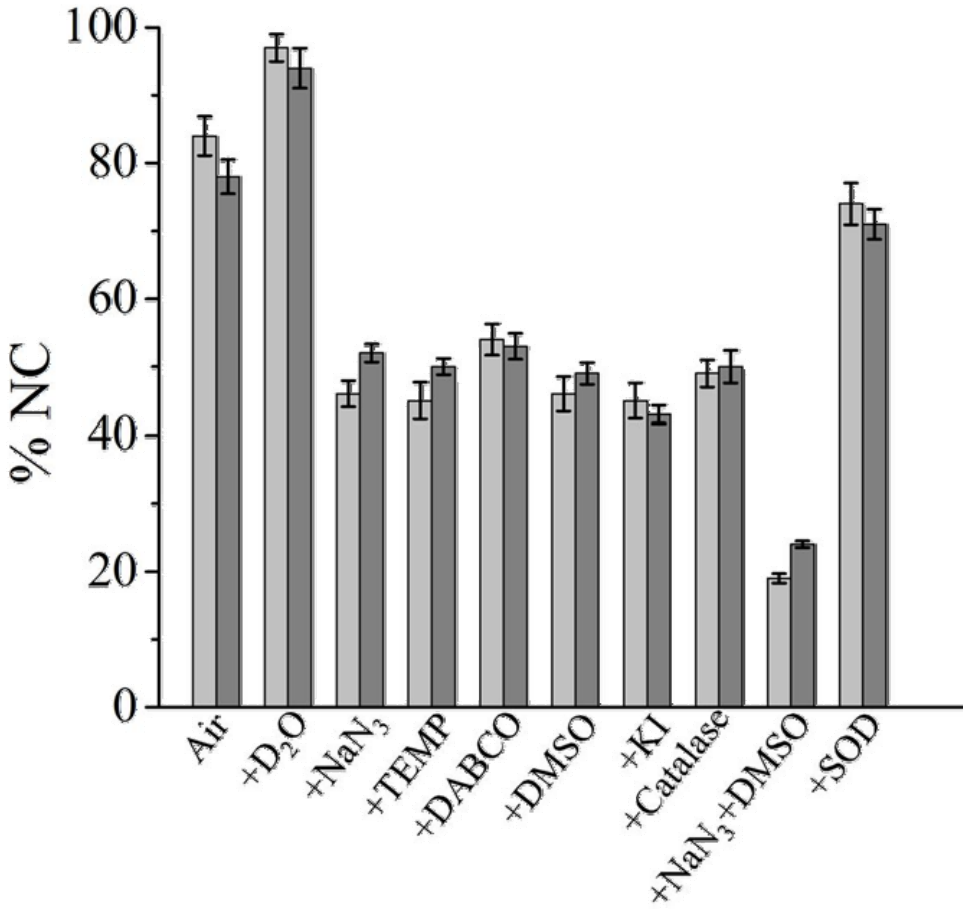

Fig. S29 A bar diagram showing the cleavage of SC pUC19 DNA (0.2 μg, 30 μM) by [Gd(py-tpy)(cur)$(NO_3)_2$] (**6,** light shade) and [Gd(py-tpy)(scur)$(NO_3)_2$] (**8,** dark shade) in UV-A light of 365 nm (6 W) in the presence of various additives in Tris-HCl buffer containing 10% DMF. The complex concentration and exposure time are 1.0 μM and 2 h, respectively. The additive concentrations/quantities are: sodium azide, 0.5 mM; KI, 0.5 mM; TEMP, 0.5 mM; DABCO, 0.5 mM; D_2O, 16 μL; DMSO, 4 μL; catalase, 4 units and SOD, 4 units.

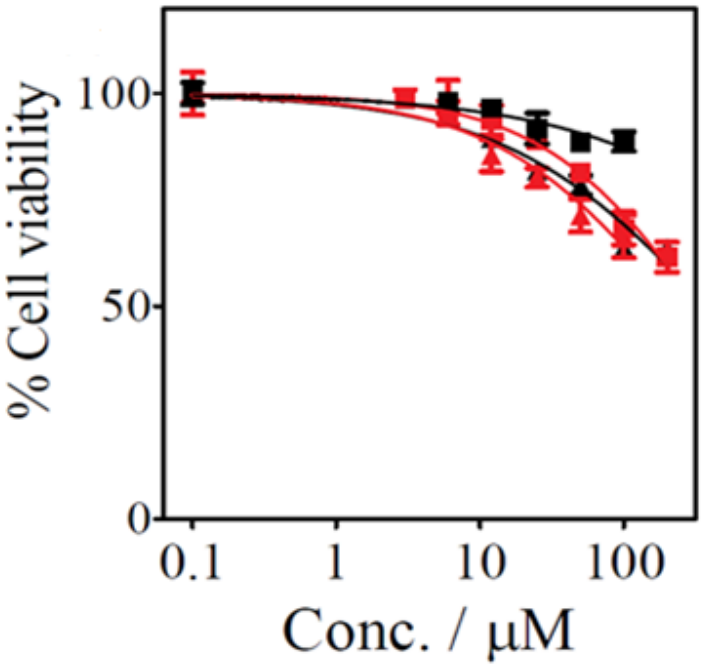

Fig. S30 Cell viability plots showing the photocytotoxicity of the ph-tpy (red squares in light and black squares in dark) and py-tpy (red triangles in light and black triangles in dark) in HeLa cells on 4 h incubation in dark followed by exposure to visible light (400-700 nm, 10 J cm^{-2}) for 1 h, as determined from the MTT assay.

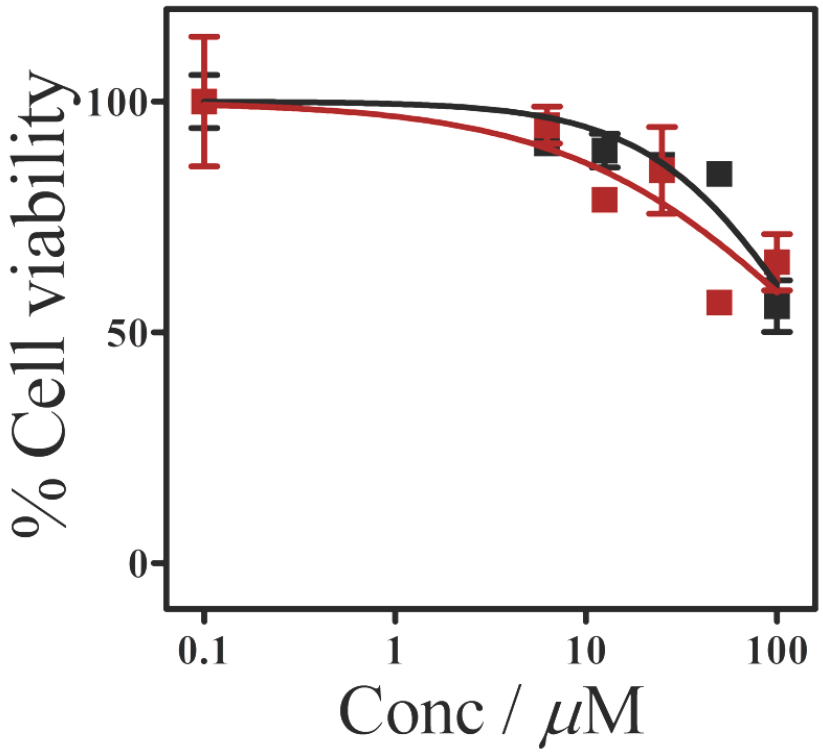

Fig. S31 Cell viability plots showing the photocytotoxicity of the Hscur ligand (red squares in light and black squares in dark) in HeLa cells on 4 h incubation in dark followed by exposure to visible light (400-700 nm, 10 J cm^{-2}) for 1 h, as determined from the MTT assay.

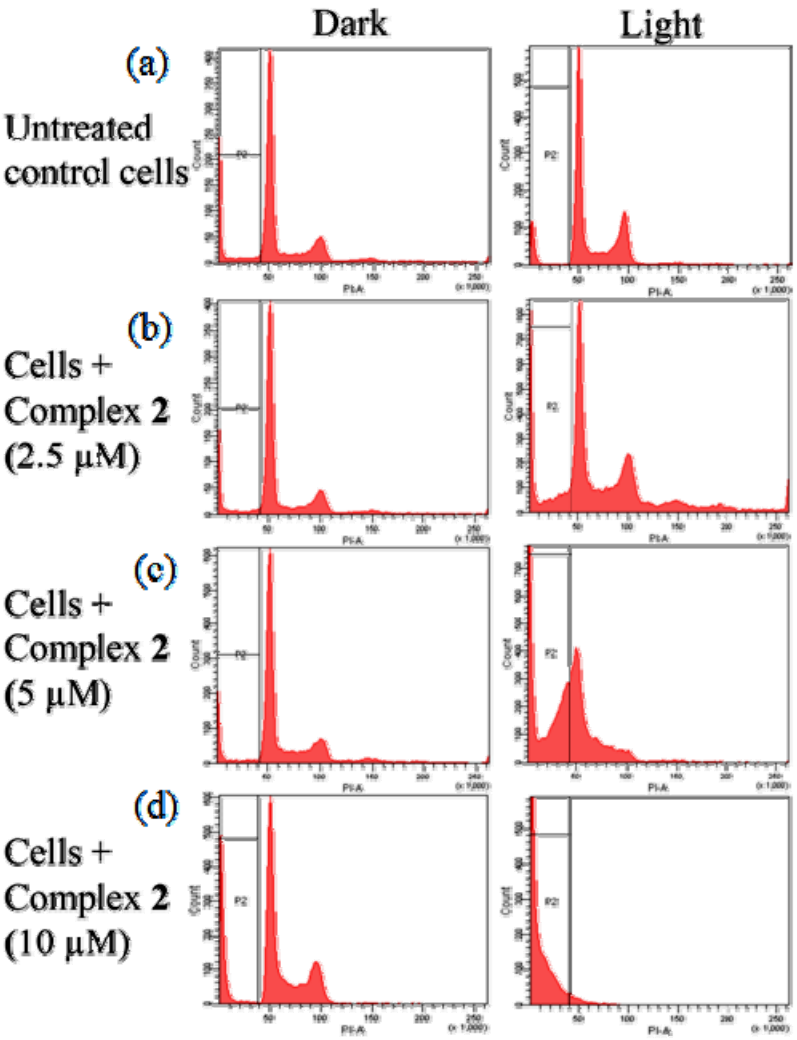

Fig. S32 Apoptotic cell death induced by complex **2** from flow cytometric analysis (photo-exposure time = 15 min, incubation time = 24 h).

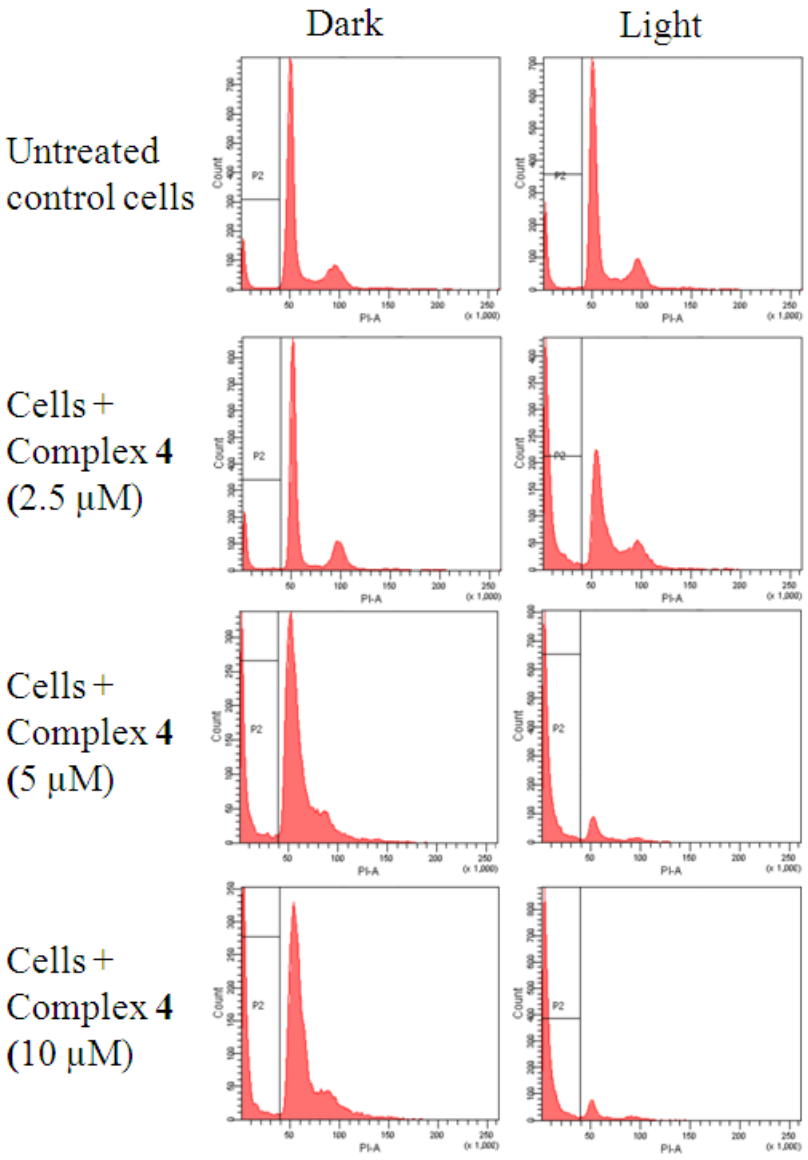

Fig. S33 Apoptotic cell death induced by complex **4** from flow cytometric analysis (photo-exposure time = 15 min, incubation time = 24 h).

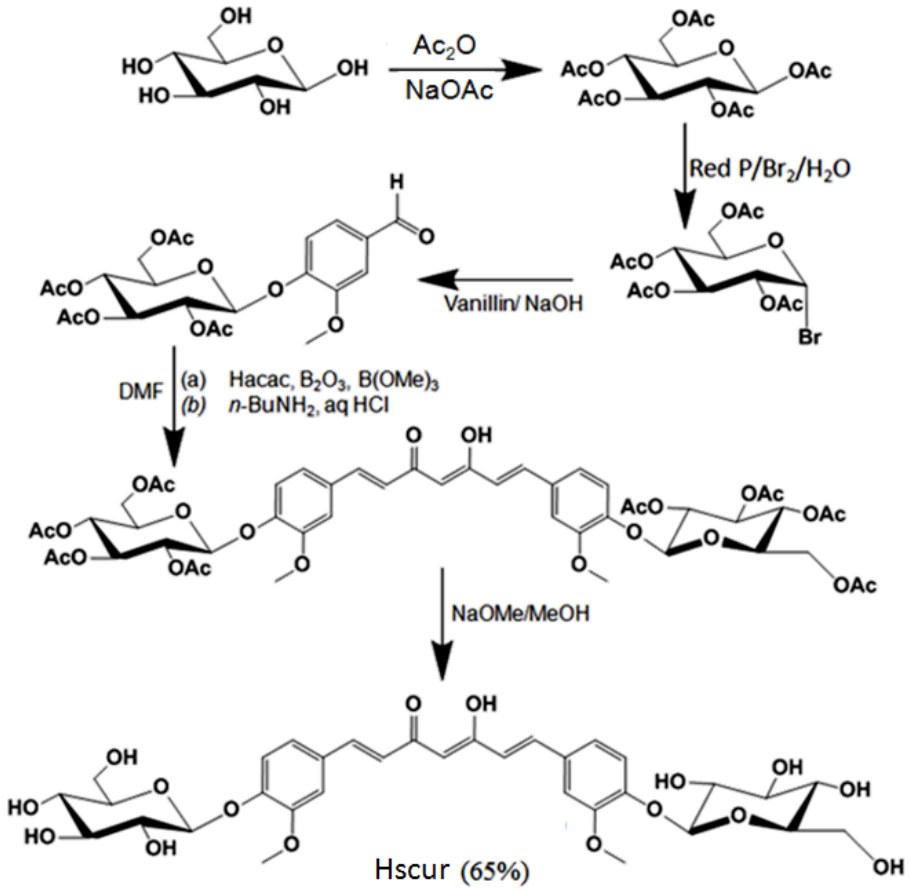

Fig. S34 Reaction scheme and the reagents used for the synthesis of diglucosylcurcumin (Hscur) ligand.